Macromolecules

pubs.acs.org/Macromolecules Article

Precise Isotactic or Atactic Pendant Alcohols on a Polyethylene Backbone at Every Fifth Carbon: Synthesis, Crystallization, and Thermal Properties

Gina A. Guillory, Stephanie F. Marxsen, Rufina G. Alamo, and Justin G. Kennemur*

Cite This: *Macromolecules* 2022, 55, 6841−6851 Read Online

ACCESS | Metrics & More | Article Recommendations | Supporting Information

ABSTRACT: A semi-crystalline precision polymer with a high molar mass (>100 kg mol^{-1}), a moderate dispersity (∼1.6), and an isotactic alcohol pendant on each and every fifth carbon of a linear polyethylene backbone is synthesized through highly regioregular ring-opening metathesis polymerization of (*S*) or (*R*)-3-(*tert*-butyldimethylsiloxy)cyclopentene followed by olefin hydrogenation and alcohol deprotection. The thermal and semi-crystalline properties of these materials are compared to analogues with atactic alcohol pendants and varying degrees of head-to-tail (HT) regioregularity. For atactic polymers with HT from 77 to 99%, the change in glass transition temperature (T_g) is minimally affected (47 ± 2 °C), but the crystalline melting temperature (T_m) increases substantially from 96 to 137 °C. When highly isotactic alcohol pendant groups are present (90% enantiopure monomer and HT = 96%), the T_g increases slightly to ∼53 °C, but the T_m increases dramatically to 190 °C. Although the wide-angle X-ray diffraction patterns of atactic and isotactic materials are similar and infer equivalent crystal unit cell packing, the isotactic sample develops ∼40% crystallinity, which is double that observed for an atactic sample (20%) with high HT = 99%. The thermal stability of all samples was >360 °C. Such investigations present unexplored insights on how isotactic and precision microstructure affect material properties of polymeric systems outside the two-carbon branch periodicity of isotactic polymers from vinyl monomers. Synthesis, structural characterizations, thermal properties in addition to intermolecular hydrogen bonding, and other crystalline structural data are discussed comparatively based on tacticity.

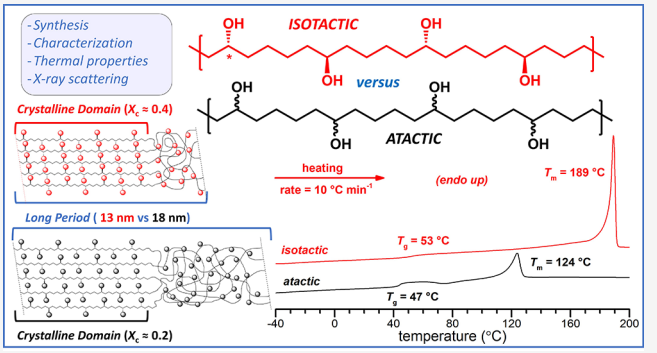

INTRODUCTION

Precision functionalized polyolefins that feature control over branch placement, composition, and stereochemistry remain a major synthetic challenge and a gateway to fundamental understanding of structure−property relationships.[1] It is well known that polymer microstructure is intimately correlated to the resulting material properties and potential applications. Aside from tremendous advances in precise control over polyolefins from vinyl monomers (i.e., a two-carbon pendant periodicity),[2−11] ring-opening metathesis polymerization (ROMP) and acyclic diene metathesis (ADMET) polymerization are well-established methods to produce precision polyolefins that feature a wide range of functionalities at varying distances along a polyolefin backbone.[12−16] In many cases, exact functional group periodicity can be pre-designed by the size and substituent locations of the monocyclic olefin or *α*-*ω*-linear diene used, respectively. To ensure precise pendant distances along the hydrocarbon backbone, symmetric and achiral monomers are often used to ensure that inconsistencies in regioregular insertion during propagation maintain precision.[13,17−19] As a result, achieving isotacticity from precision polyolefins made through ROMP, and particularly ADMET, has been a significant challenge.[13,18]

Hillmyer and co-workers discovered that allylic substituents placed on cyclooctene (COE) monomers have the ability to govern the direction of insertion on Ru-based (Grubbs) catalysts which led to highly regioregular head-to-tail (HT) polymers.[20] Computational efforts by Martinez et al. determined that the energetic pathway for propagation favored a distal insertion direction which was influenced by the steric bulk of the allylic substituent on COE and the metallacyclobutane intermediate.[21] Zhang et al. later produced enantiopure allylic acetate COE to create one of the first isotactic polyoctenamers.[22] Since that time, various allylic substituents, such as ethers,[23] ferrocenes,[24] amides,[25] tertiary amines,[26] and amino acids,[27] have been reported to produce

Received: May 25, 2022
Revised: July 1, 2022
Published: July 22, 2022

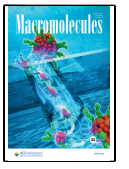

https://doi.org/10.1021/acs.macromol.2c01090
Macromolecules 2022, 55, 6841−6851

highly regioregular materials but tacticity was not explored. Di- and trisubstituted COE monomers have also led to sequence stereospecific polymers.[28] Inspired by these discoveries, our group explored regioinsertion outcomes from various allylic substituted cyclopentene (CP) derivatives during ROMP and discovered that bulky allylic trialkylsiloxy groups result in >95% HT insertion onto readily available Grubbs catalysts, such as the Hoveyda−Grubbs second generation catalyst (HG2, Umicore M720).[29−31] The choice of HG2 is due to its discovered ability to propagate these monomers at the cold temperatures (<0 °C) required for higher conversions of low-strain monomers.[17,30] Although the bulk of the allylic substituent is essential for regioregular insertion, it is also antagonistic toward chain packing of the resulting polypentenamers, resulting in amorphous materials and preventing identification of structure−property relationships on the effects of tacticity on semi-crystalline properties.[29,30]

We envisioned that post-polymerization modification to restore the alcohol functionalities by removing the trialkylsilyl protecting groups would result in precision polymers that mirror ethylene vinyl alcohol (EVOH) copolymers, which receive significant industrial interest due to their oxygen/moisture barrier properties.[32] Along with mild saturation of the backbone olefins, these materials would uniquely feature an atactic or isotactic pendant alcohol at every fifth carbon along a linear polyethylene backbone. Such structures, which could be considered with several names [e.g., poly(ethylene-*per*-vinyl alcohol-*per*-methylene), poly(ethylene-*alt*-(vinyl alcohol-*alt*-methylene), or poly(1-pentamethylene alcohol)] are unable to be produced from the copolymerization of typical vinyl and/or diene monomers.[33]

Utilization of ROMP and ADMET to produce EVOH inspired materials has received significant interest (Scheme 1). Early work by Ramakrishnan and Chung produced statistically distributed alcohol pendant groups on polyalkenamers through organoborane chemical modification.[34,35] Notably the hydroboration-oxidation of backbone olefins on a polypentenamer produced a material with dyad distributions of atactic 1,5-, 1,6-, and 1,7-diols resulting in a glass transition temperature (T_g) of 45 °C and a crystalline melting temperature (T_m) of 103 °C.[35] A similar T_g value was later reported by Herz et al.[36] Early work from Grubbs and co-workers presented a series of atactic and also stereoregular EVOH derivatives.[37−39] Scherman et al. produced well-defined poly[(vinyl alcohol)$_2$-*alt*-methylene] through ROMP of strained sila-bicyclo monomers that could be desilylated to vicinal *cis*-diols on a linear five-carbon repeating unit.[38] These can be likened to a EVOH copolymer with 80% vinyl alcohol (VOH) and the resulting T_m was shown to increase to 193 °C,[38] similar to atactic EVOH materials with similar VOH content.[33] Here we note that although stereoregularity was well-defined within the diols of a single repeating unit, racemic diads were present, which reduce the overall tacticity throughout the length of the polymer chain.[38] Similarly, *cis*- or *trans*-vicinal diols on a polyoctenamer backbone (50% VOH) were produced through deprotection of acetonide pendants on a polymerized COE monomer and displayed lower T_g (34−50 °C) and T_m (111−157 °C) values.[39] ADMET has also produced several precision EVOH materials with atactic alcohols separated by a homologous series of methylene units.[40−43] In general, the T_m decreased from 145 to 120 °C with decreasing VOH content of 44−22%, respectively.[40,41] Interestingly, in precision materials with larger hydrocarbon "runs" of 14 and 20 methylene units between the alcohol pendants, the T_m remained relatively constant (126 ± 2 °C), suggesting that increasing length of the polyethylene spacer past a certain amount no longer played a large role in thermal behavior.[43] Recently, Tuba and Grubbs reported direct ROMP of achiral and symmetric 3-cyclopenten-1-ol to produce precision atactic EVOH materials (40% VOH).[44] However, direct polymerization of the alcohol functional group led to low molecular weight polymers (<5 kg mol^{-1}), possibly due to complications in solubility, and thermal properties were not reported.

Scheme 1. Periodic Alcohol Pendants on Polyethylene Backbones Produced from ROMP or ADMET

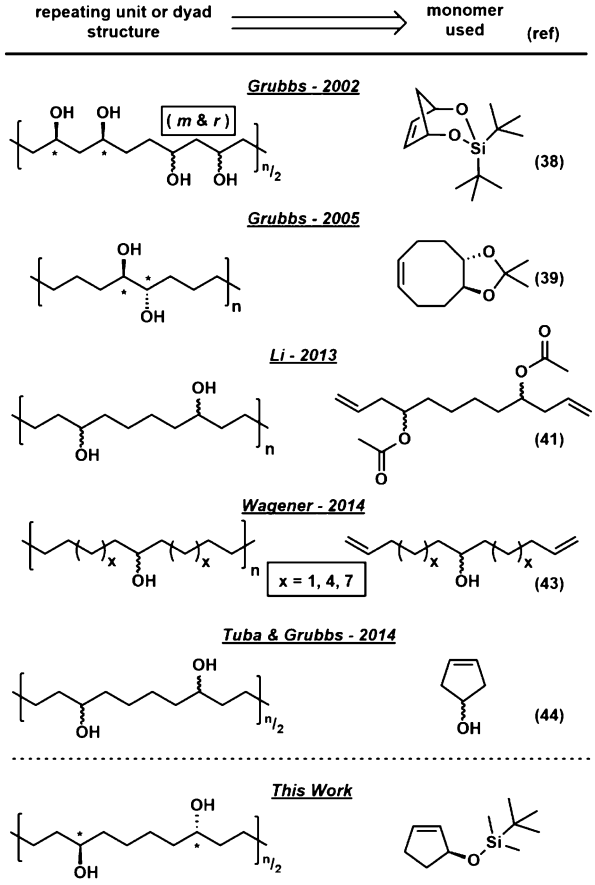

Despite the success in synthesizing a variety of precision EVOH materials from ADMET and ROMP, achieving highly isotactic stereochemistry along with precise alcohol pendant placement throughout the length of a linear backbone remains unprecedented (Scheme 1). Herein, we report the first semi-crystalline material from a polypentenamer that features an isotactic alcohol pendant group attached at every fifth carbon along a polyethylene backbone following hydrogenation of the olefins. We explore the effect of regioregularity and tacticity on the semi-crystalline properties. Such investigations present new knowledge of how isotactic and precision microstructure affect material properties of polymeric systems outside the two-carbon pendant periodicity.

EXPERIMENTAL SECTION

Materials. All chemicals were used as received unless otherwise specified. Acetone (98%), acetonitrile (MeCN, 98.5%), dimethyl sulfoxide (DMSO, 99.9%), hexane (98.5%), hydrochloric acid (HCl, 36−38% in water), magnesium sulfate ($MgSO_4$, 99%), sodium bicarbonate ($NaHCO_3$, 99.7%), potassium bicarbonate ($KHCO_3$,

https://doi.org/10.1021/acs.macromol.2c01090
Macromolecules 2022, 55, 6841−6851

99.7%), and sodium chloride (NaCl, >99.9%) were purchased from VWR. Acetyl chloride (98%), basic alumina (100%), and ethyl vinyl ether (EVE, 99%) were purchased from Alfa Aesar. Butylated hydroxytoluene (BHT, Aldrich, 99%), *N*,*N*′-dicyclohexylcarbodiimide (DCC, 99%), 4-dimethylaminopyridine (DMAP, 99%), (*R*)-(+)-α-methoxy-α-trifluoromethylphenylacetic acid (99%), *o*-xylene (98%), and tributylamine (TBA, 98.5%) were purchased from Sigma-Aldrich. Cyclohexane (99%), dichloromethane (DCM, 99%), diethyl ether (DEE, 99%), ethyl acetate (99%), and methanol (MeOH, 99%) were purchased from Millipore. *tert*-Butyldimethylchlorosilane (TBS-Cl, 99%), tetrabutyl ammonium fluoride hydrate (TBAF-H_2O, 98%), tris(dibenzylideneacetone)-dipalladium(0)-chloroform ($Pd_2(dba)_3CHCl_3$, 98%), (1*R*, 2*R*)-*trans*-1,2-diaminocyclohexane (97%), *p*-toluene sulfonyl hydrazide ($TsNHNH_2$, 95%), imidazole (99%), pyridine (99%) *N*-bromosuccinimide (NBS, 98%), (1*S*, 2*S*)-*trans*-1,2-diaminocyclohexane (98%), and 2-(diphenylphosphanyl)-benzoic acid (97%) were purchased from Oakwood Chemical. Deuterated chloroform ($CDCl_3$, 99.8%) and deuterated dimethyl sulfoxide (DMSO-d_6, 99.9%) were obtained from Cambridge Isotope Labs. 1-Ethyl-3-(3-dimethylaminopropyl)carbodiimide (EDCl, 95%) was obtained from OxChem. Silica gel (93%) was obtained from Sorbtech. Benzene (99%) was obtained from Beantown Chemical. Azobisisobutyronitrile (AIBN, Aldrich, 98%) was recrystallized from methanol and dried under vacuum prior to use. Anhydrous solvents of dimethylformamide (DMF), tetrahydrofuran (THF), toluene, and DCM were obtained from an SG Waters glass contour solvent purification system and the solvents were passed through a 2 μm filter before being dispensed. The Hoveyda−Grubbs second generation catalyst (HG2, Umicore M720) was either purchased from Sigma-Aldrich or generously donated by Umicore and used as received.

Characterizations. ^{1}H and ^{13}C NMR experiments were taken on Bruker Avance III 400 and 600 MHz spectrometers, respectively. Optical rotation was determined on samples of known concentration at 25 °C using a JASCO P-2000 polarimeter with a 589 nm wavelength filter and a quartz cell (1 dm path length). Optical rotations were acquired after a minimum of five scans to determine signal stability. Polymers were characterized on an Agilent−Wyatt combination triple detection size exclusion chromatography (SEC) instrument containing three successive Agilent PL gel Mixed-C columns (THF mobile phase), and an Agilent 1260 infinity series pump, degasser, autosampler, and thermostatted column chamber. The Wyatt triple detection unit hosts a mini-DAWN TREOS three-angle light scattering detector, Optilab TrEX refractive index detector, and a ViscoStar II differential viscometer. Number average molar mass (M_n) and dispersities (Đ) were determined by a 10-point conventional column calibration with narrow dispersity polystyrene standards varying from 2 to 1800 kDa. A Perkin Elmer Spectrum 100 Fourier transform infrared spectrometer on attenuated total reflectance (ATR) mode was used to collect IR spectra. The ATR stage is equipped with a ZnSe crystal overcoated with a diamond surface.

Differential scanning calorimetry (DSC) was conducted with a TA Q2000 equipped with an RC900 intracooler to allow subambient temperature control and operated under dry nitrogen gas. Static temperature and heat of fusion were calibrated with indium. Thermal properties of the materials were investigated by heating to 210 °C and holding isothermally for 5 min to erase thermal history before cooling to −50 °C and subsequently heating to 210 °C at 10 °C min^{-1} to observe crystallization and melting thermograms. Thermogravimetric analysis (TGA) was performed on a TA Instruments TGA-550 instrument under argon flow (50 mL min^{-1}). Samples were heated to 100 °C, held isothermally for 5 min and then heated to 550 °C at a rate of 10 °C min^{-1}.

Small-angle X-ray scattering (SAXS) and wide-angle X-ray diffraction (WAXD) patterns were collected simultaneously at room temperature on a Bruker Nanostar diffractometer with an Incoatec microfocus X-ray source (Iμs). The incident X-ray beam was a Cu Kα line with a wavelength of 1.5418 Å. The instrument is equipped with a HiStar 2D Multiwire SAXS detector and a Fuji Photo Film plate which is read with a Fuji FLA-7000 scanner used for WAXD detection. Samples were prepared for analysis by isothermal crystallization in DSC at selected T_c values of 116 and 170 °C for atactic and isotactic samples, respectively. About 4 mg of a ∼50 μm thick film was encapsulated in Al DSC pans and samples were held isothermally at 210 °C for 5 min followed by subsequent cooling at 40 °C min^{-1} to T_c. Each sample was held isothermally at T_c for enough time to allow the exothermic crystallization peak to complete and then were cooled at 40 °C min^{-1} to room temperature. After thermal treatment, samples were removed from the DSC pans and analyzed within the X-ray scattering instrument.

Synthesis. *rac*-2-cyclopenten-1-ol (1). To a 500 mL round-bottom flask (RBF), equipped with a polytetrafluoroethylene (PTFE) coated stir bar, 40 mL (435 mmol) of CP, 73.45 g (409 mmol, 0.94 mol equiv) of NBS, and 0.04 g (0.24 mmol) of AIBN were dissolved in 200 mL cyclohexane. The reaction mixture was stirred at 80 °C for 3 h. The reaction was quenched by cooling to 0 °C and the solids removed via vacuum filtration. After concentration via rotary evaporation, the crude 3-bromocyclopentene and 33.5 g (398 mmol, 0.92 mol equiv) of $NaHCO_3$ were dissolved in 400 mL of an acetone/water mixture (2:1 v/v). The reaction mixture was allowed to stir under reflux for 2 h. The solids were removed via vacuum filtration and the reaction mixture was concentrated via rotary evaporation. The product was extracted with 3 × 50 mL of DEE, dried over $MgSO_4$, and concentrated via rotary evaporation. The crude brown oil was distilled under reduced vacuum (50 °C, 4 torr), to afford 7 g (55 mmol, 19%) of **1** as a colorless liquid. Characterization by NMR spectroscopy was consistent with the literature.[22,30]

^{1}H NMR (400 MHz, $CDCl_3$): δ(ppm) 5.99 (dtd, *J* = 5.6, 2.2, 1 Hz, 1H), 5.89−5.80 (m, 1H), 4.87 (dddt, *J* = 7.9, 3.3, 2.1, 1.0 Hz, 1H), 2.56−2.54 (m, 1H), 2.30−2.20 (m, 2H), 1.74−1.64 (m, 1H), 1.52−1.46 (s, 1H). ^{13}C NMR (150 MHz, $CDCl_3$): δ(ppm) 135.10, 133.32, 77.58, 33.31, 30.96.

***rac*-3-(*tert*-butyl-dimethylsiloxy)cyclopentene (2).** To a 500 mL RBF, equipped with a PTFE stir bar, 4 g (47.6 mmol) of **1** and 13.8 (190 mmol, 4 mol equiv) imidazole was dissolved in 300 mL anhydrous DCM. The solution was cooled to 0 °C, and 8.6 g (57.2 mmol, 1.2 mol equiv) of TBS-Cl was added in 2.5 g portions. The reaction stirred at 23 °C for 15 min, before heating to reflux for 14 h. The reaction was then cooled to 0 °C and diluted with 100 mL DCM. The solids were removed via vacuum filtration and the organic filtrate was washed with 3 × 100 mL water in a separatory funnel. The organic layer was collected, dried over $MgSO_4$, and concentrated via rotary evaporation. The crude product was purified via column chromatography with a mobile phase of 100:5 v/v hexane/DCM to afford 6 g (30.2 mmol, 63.6%) of **2** as a colorless liquid. Characterization by NMR spectroscopy was consistent with the literature.[29]

^{1}H NMR (400 MHz, $CDCl_3$): δ(ppm) 5.92 (dtd, *J* = 5.7, 2.2, 1.2 Hz, 1H), 5.74 (dq, *J* = 5.7, 2.1 Hz, 1H), 4.94 (dddt, *J* = 7.1, 3.7, 2.4, 1.2 Hz, 1H), 2.57−2.43 (m, 1H), 2.31−2.15 (m, 2H), 1.68 (ddt, *J* = 12.6, 9.2, 4.8 Hz, 1H), 0.92 (s, 9H), 0.11 (s, 6H). ^{13}C NMR (150 MHz, $CDCl_3$): δ(ppm) 133.87, 133.50, 78.13, 77.22, 77.01, 76.80, 33.53, 31.01, 26.00, 25.71, 18.33, 18.13, −2.94, −4.53, −4.56.

***rac*-cyclopent-2-en-1-yl acetate (3).** To a 500 mL RBF, equipped with a PTFE coated stir bar, 4.6 g (54.7 mmol) of **1**, 6.63 mL (82 mmol, 1.5 mol equiv) of pyridine and 1.67 g (13.7 mmol, 0.25 mol equiv) of DMAP was dissolved in 150 mL anhydrous DCM. The solution was sparged with Ar for 25 min and cooled to 0 °C. Dropwise, 7.78 mL (109 mmol, 2 mol equiv) of acetyl chloride was added. The reaction was allowed to stir for 14 h, then diluted with 100 mL DCM. The solution was then added to a separatory funnel and washed 3 × 50 mL with 1 M HCl, 1 × 50 mL with sat. $NaHCO_3$ solution, and 1 × 50 mL with brine. The organic layer was collected, dried over $MgSO_4$, and concentrated via rotary evaporation. The crude product was purified by column chromatography with a mobile phase of 100:1 v/v hexane/ether to afford 3.25 g (25.7 mmol, 47%) of **3** as a pale yellow liquid. Characterization by NMR spectroscopy was consistent with the literature.[22,30]

^{1}H NMR (400 MHz, $CDCl_3$): δ(ppm) 6.16−6.09 (m, 1H), 5.84 (dq, *J* = 6.2, 2.2 Hz, 1H), 5.76−5.67 (m, 1H), 2.53 (dddt, *J* = 15.3,

https://doi.org/10.1021/acs.macromol.2c01090
Macromolecules 2022, 55, 6841−6851

Scheme 2. Synthesis of Atactic and Isotactic Polymers with a Pendant Alcohol at Every Fifth Carbon

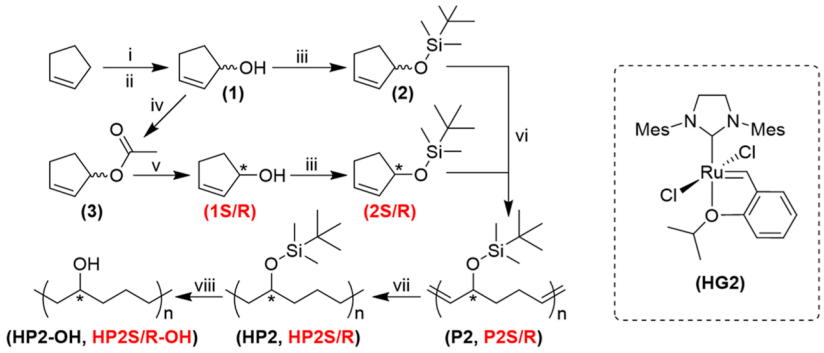

*Denotes a specific *R* or *S* stereocenter. (i) NBS, AIBN, cyclohexane, 3 h, 80 °C. (ii) $NaHCO_3$, acetone:H_2O (2:1), reflux, 2 h. (iii) TBS-Cl, imid., DCM, reflux, 14 h. (iv) acetyl chloride, pyr., DCM, 24 °C, 14 h. (v) DACH-phenyl Trost ligand, $Pd_2(dba)_3$ $CHCl_3$, $KHCO_3$, DCM, 3 °C, 48 h. (vi) HG2, tol., −15 °C, 5 h. (vii) $TsNHNH_2$, TBA, *o*-xyl., 120 °C, 8 h. (viii) TBAF (1 M), THF:DMF (3:1), 55 °C, 48 h.

10.8, 5.2, 4.8, 2.2 Hz, 1H), 2.41−2.21 (m, 2H), 2.05 (s, 3H), 1.84 (ddt, *J* = 13.8, 12.2, 3.3 Hz, 1H). ^{13}C NMR (150 MHz, $CDCl_3$): δ(ppm) 171.05, 137.55, 129.27, 80.48, 31.06, 29.77, 21.32.

***(S)*-2-cyclopenten-1-ol (1S).** (*R*,*R*)-DACH-phenyl Trost ligand was freshly synthesized according to the literature (Supporting Information).[45,46] To a flame-dried RBF, equipped with a PTFE stir bar, 0.88 g of (*R*,*R*)-DACH-phenyl Trost ligand (1.27 mmol, 0.08 mol equiv), 0.66 g of $Pd_2(dba)_3CHCl_3$ (0.64 mmol, 0.04 mol equiv), and 2.22 g (22.2 mmol, 2.2 mol equiv) of $KHCO_3$ were added under Ar. Degassed DCM (250 mL) was transferred into the round bottom via cannulation and the solution was allowed to stir at 23 °C for 15 min followed by cooling to 3 °C. Separately, 2 g (15.9 mmol) of **3** was dissolved in 2 mL of anhydrous DCM and sparged with Ar for 10 min. The solution of **3** and 30 mL of Ar-sparged water were added simultaneously with separate syringes and the reaction was allowed to stir at 3 °C for 24−48 h. Conversion was determined periodically using thin layer chromatography with a mobile phase of 100:5 v/v DCM/MeOH. The reaction mixture was then filtered via vacuum filtration and then concentrated via rotary evaporation. The crude product was purified via column chromatography with a mobile phase of 100:5 v/v DCM/MeOH to afford 0.74 g (8.8 mmol, 55.7%) of **1S** as a colorless liquid. The specific optical rotation $[\alpha]_{25}^{589}$ = −110.1° (±3.4°) was determined and indicates an enantiopurity of ∼93% from the literature.[47] Characterization by NMR spectroscopy was consistent with the literature.[30]

^{1}H NMR (500 MHz, $CDCl_3$): δ 6.01 (ddq, *J* = 5.7, 2.4, 1.1 Hz, 1H), 5.85 (dt, *J* = 5.7, 2.2 Hz, 1H), 4.92−4.84 (m, 1H), 2.58−2.47 (m, 1H), 2.35−2.23 (m, 2H), 1.76−1.64 (m, 1H), 1.56 (s, 1H). ^{13}C NMR (150 MHz, $CDCl_3$): δ(ppm): 135.18, 133.29, 77.62, 33.31, 30.97.

***(S)*-3-(*tert*-butyl-dimethylsiloxy)cyclopentene (2S).** The same synthetic procedure to produce **2** from **1** was used to produce **2S** from **1S** with the following differences: 2.79 g (18.5 mmol, 1.2 mol equiv) of TBS-Cl was added to 1.3 g (15.5 mmol) of **1S** and 4.25 g (61.6 mmol, 4 mol equiv) of imidazole in 150 mL DCM. Yield: 2.40 g (12.1 mmol, 78.2%). $[\alpha]_{25}^{589}$ = −85.8° (±1.8°).

^{1}H NMR (500 MHz, CDCl3): δ 5.92 (dtd, *J* = 5.8, 2.2, 1.2 Hz, 1H), 5.74 (dq, *J* = 5.7, 2.0 Hz, 1H), 4.94 (ddtd, *J* = 8.9, 4.4, 2.2, 1.3 Hz, 1H), 2.57−2.42 (m, 1H), 2.29−2.16 (m, 2H), 1.73−1.61 (m, 1H), 0.92 (s, 10H), 0.11 (s, 7H). ^{13}C NMR (150 MHz, $CDCl_3$): δ(ppm): 133.87, 133.47, 78.12, 33.52, 30.99, 25.99, 18.31, −4.55, −4.57.

***(R)*-2-cyclopenten-1-ol (1R).** The same synthetic procedure to produce **1S** from **3** was used to produce **1R** from **3** with the following differences: 1.31 g (1.9 mmol, 0.08 mol equiv) of (*S*,*S*)- DACH-phenyl Trost ligand (Supporting Information), 0.99 g (0.95 mmol, 0.04 mol equiv) of $Pd_2(dba)_3$, and 5.25 g (50.2 mmol, 2.2 mol equiv) of $KHCO_3$ was dissolved in 300 mL anhydrous DCM. Then, 3 g of **3** (24 mmol) and 50 mL of sparged DI water were added. Yield: 0.3 g (3.5 mmol, 15% yield). $[\alpha]_{25}^{589}$ = 111.5° (±0.32°) was determined and indicates an enantiopurity of ∼93% from the literature.[47]

^{1}H NMR (400 MHz, $CDCl_3$): δ(ppm) 6.01 (ddq, *J* = 5.6, 2.2, 1.0 Hz, 1H), 5.85 (dt, *J* = 5.4, 2.2 Hz, 1H), 4.89 (dtd, *J* = 7.0, 2.3, 1.1 Hz, 1H), 2.53 (dddd, *J* = 16.6, 8.0, 4.1, 1.7 Hz, 1H), 2.38−2.22 (m, 2H), 1.71 (tq, *J* = 12.8, 4.1 Hz, 1H). ^{13}C NMR (150 MHz, $CDCl_3$): δ(ppm) 135.12, 133.31, 77.61, 33.33, 30.95.

***(R)*-3-(*tert*-butyl-dimethylsiloxy)cyclopentene (2R).** The same synthetic procedure to produce **2S** from **1S** was used to produce **2R** from **1R** with the following differences. 0.65 g (4.3 mmol, 1.2 mol equiv) of TBS-Cl was added to 0.3 g (3.6 mmol) of **1R** and 0.98 g (14.3 mmol, 4 mol equiv) of imidazole in 100 mL of anhydrous DCM. Yield: 0.5 g (2.5 mmol, 70.8% yield). $[\alpha]_{25}^{589}$ = 85.4° (±1.2°).

^{1}H NMR (400 MHz, $CDCl_3$): δ(ppm) 5.92 (dq, *J* = 5.9, 2.0 Hz, 1H), 5.74 (dq, *J* = 5.9, 2.1 Hz, 1H), 4.93 (ddd, *J* = 6.8, 4.2, 2.0 Hz, 1H), 2.50 (dddd, *J* = 12.9, 9.5, 4.7, 2.3 Hz, 1H), 2.32−2.13 (m, 2H), 1.68 (ddt, *J* = 13.6, 9.2, 4.8 Hz, 1H), 0.92 (s, 9H), 0.10 (s, 6H). ^{13}C NMR (150 MHz, $CDCl_3$): δ(ppm) 133.88, 133.47, 78.12, 33.53, 30.99, 25.99, 18.30, −4.54, −4.56.

Polymerizations. All ROMP was performed in accordance with the general procedure for **P2** described here. To an oven-dried 20 mL vial, equipped with a PTFE stir bar, 9.2 mg (0.0147 mmol) of HG2 was added. The vial was sealed with a septum, purged with Ar, and 2−3 drops of anhydrous toluene was injected to dissolve the catalyst. The vial was then injected with 5.5 g (27.7 mmol) of **2** (initial monomer to catalyst ratio, $[M]_0/[I]_0$ = 1900). The polymerization was cooled to −15 °C and stirred for 5 h. The viscous polymerization solution was then quenched with an injection of 0.2 mL of EVE followed by additional stirring at −15 °C for 12 h. A crude aliquot was taken to determine percent monomer conversion (52%) by ^{1}H NMR ($CDCl_3$) through comparative integration of the monomer (5.90−5.94 ppm) and polymer (5.49−5.58 ppm) olefin proton signals (Supporting Information). The remaining polymer was warmed to room temperature and diluted in DCM. The polymer solution was passed through a basic alumina column and precipitated in MeOH. Redissolution/reprecipitation was performed twice and the polymer was collected and dried under high vacuum for 24 h to yield 2.75 g (13.8 mmol, 96% recovered based on 52% conversion) of **P2** as a colorless, gummy solid.

Hydrogenation. Hydrogenation of the backbone olefins for each polymer was performed in accordance with the general procedure described here. To a RBF, equipped with a PTFE stir bar, 2.75 g (13.8 mmol of olefins) of **P2** was dissolved in 200 mL *o*-xylene. A catalytic amount of BHT was added, along with 11.61 g (62.6 mmol, 4.5 mol equiv) of *p*-toluene sulfonyl hydrazide and 16.5 mL (69.5 mmol, 5 mol equiv) of TBA. For most samples, the reaction was allowed to reflux for 8 h, then cooled to room temperature. Later, it was discovered that reflux temperatures caused some loss of polymer molar mass and that lowering the reaction temperature to 120 °C for 8 h mitigated this issue while still allowing quantitative hydrogenation.

https://doi.org/10.1021/acs.macromol.2c01090
Macromolecules 2022, 55, 6841−6851

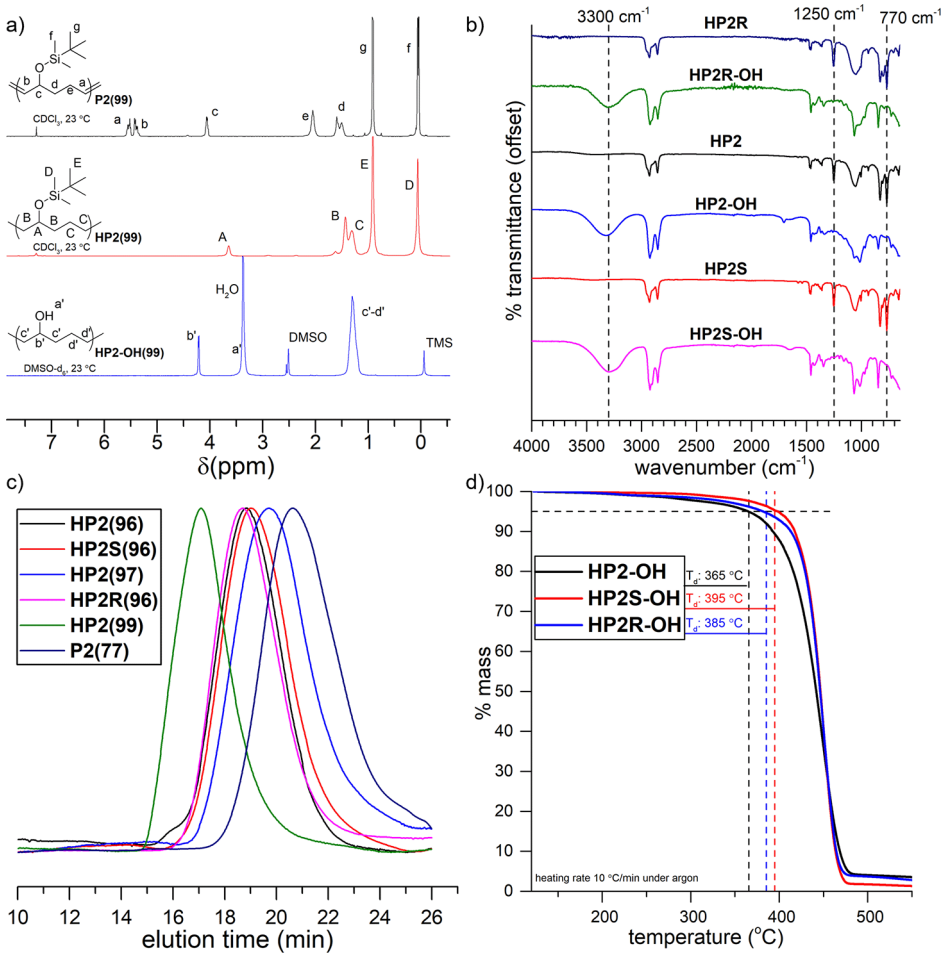

Figure 1. (a) Stacked ^{1}H NMR spectra of **P2(99)**, **HP2(99)** ($CDCl_3$, 400 MHz, 25 °C), and **HP2−OH(99)** (DMSO-d_6, 400 MHz, 25 °C). (b) Stacked ATR IR spectra of polymer samples before and after removal of TBS protecting groups. Vertical dashed lines indicate key absorptions used to conclude the presence/absence of TBS and alcohol peaks. (c) Normalized SEC refractive index signals of TBS protected polymers following hydrogenation (THF mobile phase). (d) Overlaid TGA thermograms of atactic [**HP2−OH(99)**] and isotactic [**HP2S−OH(96)** and **HP2R−OH(96)**] samples under argon (rate = 10 °C min^{-1}). Horizontal and vertical dashed lines indicate the point of 5% mass loss for each sample.

The polymer was precipitated in cold MeOH, collected, and freeze-dried in benzene overnight. This yielded 2.7 g (13.5 mmol, 97.8% recovered) of **HP2** as a viscous clear fluid.

Alcohol Deprotection. Removal of the TBS groups from each polymer was performed in accordance with the general procedure described here. To a flame-dried RBF, equipped with a PTFE stir bar, 2.7 g (13.5 mmol) of **HP2** was dissolved in 2:1 v/v mixture of anhydrous THF: DMF and heated to 55 °C. In a separate 50 mL RBF, 14.5 g (55 mmol, 4 mol equiv) of TBAF (previously dried under vacuum for 24 h at 40 °C to remove H_2O) was diluted in 55 mL of anhydrous THF and added to the polymer solution (final solvent ratio 3:1 THF/DMF). The reaction was allowed to stir for 48 h at 55 °C. The solution was then cooled, concentrated via rotary evaporation, and precipitated in acetone. The polymer was collected, redissolved in DMSO, and reprecipitated in acetone twice more to yield 0.5 g (5.8 mmol, 43% recovered) of **HP2−OH** as a fluffy/flakey white solid.

RESULTS AND DISCUSSION

For clarity of sample identification, a sample ID of **HP2S−OH(X)** indicates a polymer (**P**) that has been synthesized with enantiopure (**2S**) monomer, has been hydrogenated (**H**), and has the alcohol deprotected (**-OH**) through post-polymerization modification (Scheme 2). The number in parentheses "**X**" represents the determined percent HT regioregularity (% HT). Polymers without **R** or **S** in the sample ID indicate that a racemic monomer was used (atactic polymer). In a previous investigation, **2** (Scheme 2) was identified as an ideal monomer that results in highly regioregular propagation during ROMP (~97% HT) and has sufficient thermodynamics (equilibrium polymerization enthalpy ΔH_p and entropy ΔS_p) to produce moderate monomer conversions (50−60%) in bulk at cold temperature (−15 °C).[29] We note that these thermodynamic parameters are critical for low-strain CP monomers to obtain adequate monomer conversion in equilibrium ROMP.[17] The bulky *tert*-butyl-dimethylsiloxy (TBS) substituent, located on the allylic position of the CP monomer, is believed to preferentially insert onto the **HG2** catalyst (Scheme 2) in a distal direction, due to sterics, leading to the high HT regioregularity.[21] A high degree of *trans* backbone olefin stereochemistry (≥94%) was also determined. Similar *trans* selectivity has also been reported with allylic substituted cyclooctene derivatives.[20,22,25,48]

In this study, the synthetic path to **1** was modified utilizing a Wohl−Ziegler bromination with NBS,[49] followed by hydroxyl substitution and loss of bromide using $NaHCO_3/H_2O$/acetone solution. This route was significantly cheaper and less hazardous than the previously reported reduction of 2-cyclopentenone using DIBAL,[30] despite having less yield. The alcohol on **1** was directly protected with TBS to produce

https://doi.org/10.1021/acs.macromol.2c01090
Macromolecules 2022, 55, 6841−6851

racemic monomer, **2.** Alternatively, **1** was reacted with acetyl chloride (**3**) and subjected to dynamic kinetic resolution of allylic esters using palladium in the presence of chiral (*R,R*)− or (*S,S*)−DACH−phenyl Trost ligand to produce the enantiopure **1R** and **1S**, respectively (Scheme 2).[45,47] Both **1R** and **1S** had an enantiopurity of 91 ± 2% as determined by specific optical rotation and diastereomeric resolution using Mosher's acid (Supporting Information).[50] The chiral alcohol on **1R** and **1S** was then protected with TBS-Cl to produce the monomers **2R** and **2S**, respectively. In addition to the regioregular insertion supplied by the bulky TBS group during ROMP, alcohol protection also provides a monomer/polymer system that is easily soluble in $CHCl_3$ and THF, allowing for homogeneous polymerizations and solution characterizations.

ROMP was performed cold (−15 °C) and in near bulk conditions to maximize monomer conversion. The HG2 catalyst (Scheme 2) was used due to its adequate prior performance at cold temperature.[29,30] The polymerizations were also terminated at −15 °C with EVE to remove and suppress the activity of the Ru catalyst and prevent depolymerization upon warming and workup. Aliquots of crude polymerization solutions were analyzed by ^{1}H NMR spectroscopy to determine monomer conversions which were between 50−70%, consistent with previous reports.[29] A series of four atactic **P2** samples were synthesized and analyzed by ^{1}H NMR, ^{13}C NMR, and SEC (Figure 1a and the Supporting Information). Using a peak deconvolution analysis on the allylic methine proton signal by ^{1}H NMR, the regioregularity (%HT) and *trans* backbone olefin content were determined (Table S1).[29] For samples **P2(96)**, **P2(97)**, and **P2(99)**, the % HT was 95−99% whereas the %trans olefins was 94−97%, indicating a precise polymer microstructure. An exception is **P2(77)** which resulted in 77% regioregular insertion. The reason for the reduction in precision for **P2(77)** is unknown but is hypothesized to originate from the age of the HG2 catalyst that was used. The fresh and newly opened HG2 catalyst resulted in >95 HT % for the remaining samples. SEC analysis revealed the atactic samples to span a large range in number average molar masses (M_n) from 64 to 911 kg mol^{-1} and moderate dispersities (Đ) of 1.6−2.1 (Table S1). These large variations in molar mass were observed previously for trialkylsiloxy substituted CP monomers at cold temperature and are believed to be due to the limited initiation activity of the HG2 catalyst. Concomitantly, the consistent 50−70% monomer conversions over the course of 5 h suggest that propagation of **2** is sufficient. Notably, sample **P2(99)** presents the largest M_n (911 kg mol^{-1}) and highest %HT (99%) of any polypentenamer to date. Using identical ROMP conditions, the chiral monomers **2S** and **2R** were successfully polymerized into **P2S(96)** (M_n = 627 kg mol^{-1}, Đ = 1.5, HT = 96%) and **P2R(96)** (M_n = 427 kg mol^{-1}, Đ = 1.6, HT = 96%), respectively. Polarimetry of **P2S(96)** and **P2R(96)** in THF resulted in specific optional rotations ($[a]_{589}^{23}$) of −8.3 and +8.4°, respectively, which is notably reduced from the monomers (±83°). A reduction in $[\alpha]$ for isotactic polymers in comparison to their cycloolefin monomer is consistent with prior literature.[30,51] After purification and drying, the atactic **P2** and isotactic **P2S** and **P2R** polymers were colorless, gummy solids at room temperature.

The olefins on the backbone of each sample were quantitatively hydrogenated using tosyl hydrazide in *o*-xylene to produce a linear polyethylene backbone. Here, it was determined that 120 °C was an ideal temperature for this reaction, resulting in a complete disappearance of the olefin proton signals (5.53−5.40 ppm) and a shifting of the methine proton signal from 4.05 to 3.64 ppm by ^{1}H NMR (Figure 1a). SEC analysis before and after hydrogenation at 120 °C on sample **P2(99)** and **HP2(99)**, respectively, revealed a negligible change in retention time (Figure S42). However, performing the hydrogenation at a higher temperature (i.e., refluxing at 144 °C) quantitatively saturates the backbone but also results in variation of the polymer molar mass as determined by SEC analysis (Figures S42 and S50). No other differences to the polymer could be determined spectroscopically and the TBS groups remained present to the same extent as determined by comparative integration of the ^{1}H NMR signals (Supporting Information). Future studies will focus on a more in-depth understanding of these molar mass discrepancies which are not critical for the purposes of this study.

The hydrogenated versions of the polymers, **HP2**, **HP2S**, and **HP2R**, were subjected to alcohol deprotection using TBAF in a 3:1 v/v THF/DMF solution. Upon removal of the TBS groups, **HP2** changed from soluble in THF to insoluble in THF and soluble in DMF. Once fully dried, the white semi-crystalline **HP2−OH** would not easily redissolve in DMF, DMSO, or water at moderate temperatures (≤100 °C). Therefore, NMR analysis was performed in DMSO-d_6 after precipitation and filtration but before full drying. Figure 1a shows the ^{1}H NMR spectra of wet **HP2−OH(99)** with quantitative loss of the TBS signals (D and E). Removal of the TBS groups from **HP2** was corroborated by IR spectroscopy (Figure 1b), evidenced by the appearance of broad O−H stretches at 3500−3100 cm^{-1} and the disappearance of the Si−C stretch at 1250 and Si−O at 755 cm^{-1}. Deprotection of **HP2S** and **HP2R** resulted in materials with very low solubility once precipitated, limiting NMR analysis. However, comparative IR analysis of **HP2S** and **HP2R** to **HP2** (Figure 1b) shows nearly identical loss of silyl group signals and appearance of O−H stretching at 3300 cm^{-1} as described above. As shown vide infra, the limited solubility of the isotactic samples is likely due to a much higher propensity for them to crystallize. The resulting **HP2−OH**, **HP2S−OH**, and **HP2R−OH** samples, respectively, represent an unexplored set of materials with a linear polyethylene backbone and an atactic or isotactic alcohol pendant group on every fifth carbon.

Thermal Properties. TGA analysis was performed on representative samples under argon to measure their thermal stabilities. **P2(96)**, **HP2(96)**, and **HP2−OH(96)** had thermal decomposition temperatures (T_d), calculated at the point of 5% mass loss, of 266, 392, 365 °C, respectively (Figure S62). A notable increase in thermal stability occurs after backbone saturation and a slight reduction in stability occurs once the TBS groups are removed. **HP2−OH(96)** has a notably higher T_d than atactic poly(vinyl alcohol), PVA, which begins to lose mass ∼300 °C.[34] The T_d for isotactic **HP2S(96)-OH** and **HP2R(96)-OH** was 395 and 385 °C, respectively, which is higher than atactic **HP2(96)-OH** by 20−30 °C (Figure 1d). This increase is also similar to PVAs of varying tacticity, where isotactic derivatives had higher T_d over atactic counterparts.[52]

Polypentenamers containing the TBS functional groups were colorless gummy solids that became clear viscous fluids following hydrogenation. DSC analysis on samples before and after hydrogenation revealed a consistent T_g value of 0 ± 2 °C and −14 ± 2 °C, respectively, regardless of tacticity (Figures S58−S60). The absence of crystallinity for the

https://doi.org/10.1021/acs.macromol.2c01090
Macromolecules 2022, 55, 6841−6851

isotactic samples can be attributed to the large bulky TBS groups that prevent efficient chain packing with three-dimensional correlated symmetry. The decrease in T_g upon saturation is unique to polypentenamers with allylic substituents and typically not seen from polypentenamers with homoallylic substituents following saturation.[53] Upon deprotection and production of the alcohol functionality, the samples became white flaky solids, suggesting semi-crystalline properties. To probe this and understand the effect of %HT regioregularity on thermal properties, the atactic alcohol-functionalized samples were each analyzed by DSC at a heat/cool cycling rate of 10 °C min^{-1} under N_2. Figure 2 displays

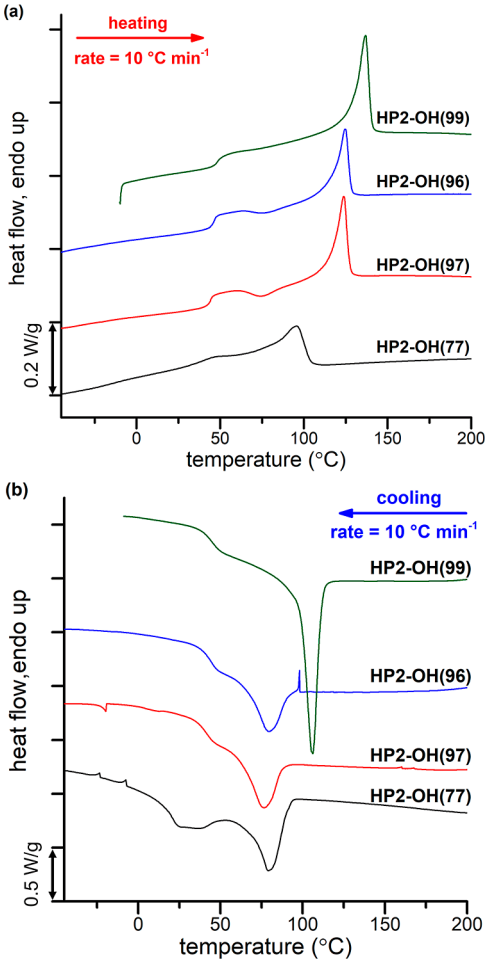

Figure 2. DSC thermograms of atactic **HP2−OH** samples upon the second cycle of (a) heating and (b) cooling at 10 °C min^{-1} under N_2. For clarity, the thermograms are shifted vertically.

the thermograms upon the second heat/cool cycle. The T_g for each sample increased following deprotection and, for M_n > 65,000 g mol^{-1}, remained relatively constant (47 ± 2 °C). However, the semi-crystalline properties, such as melting and crystallization points and heat of fusion, change in correlation with the chain microstructure. Most notably, **HP2−OH(77)**, with the lowest regioregularity, or least precise microstructure, had the lowest T_m (96 °C) and enthalpy of melting (ΔH_m = 27.5 J g^{-1}), whereas the most regioregular and precise microstructure, **HP2−OH(99)**, had the highest T_m = 137 °C and ΔH_m = 40.2 J g^{-1} (Table 1). Samples **HP2−OH(96)** and **HP2−OH(97)** had slightly lower yet fairly consistent T_m (125 and 124 °C, respectively) and ΔH_m (29.7 and 33.7 J g^{-1}, respectively), compared to **HP2−OH(99)** (Table 1). A relatively low M_n for sample **HP2−OH(77)** will also contribute to the decrease in T_g and T_m, however, based on prior polyolefin work,[54] we conclude the dramatic decrease in T_m is largely due to the poor regioregularity of this polymer. The crystallization temperatures (T_c) differ among the atactic polymers (Table 1). Because these values, along with the onset of crystallization, depend on the number density of heterogeneous nuclei, varying degrees of regioregular defects are not expected to trend accordingly. From a compositional standpoint, the unique repeating unit structure of these materials can be likened to an EVOH copolymer with 40 mol % VOH content. By comparison, the T_m reported for a statistical and atactic EVOH copolymer with ∼41 mol % VOH content is 124 °C.[33]

To compare thermal properties of atactic and isotactic samples, **HP2−OH(96)** and **HP2S−OH(96)** were used as representative samples due to their matched %HT and similar molecular weight. Figure 3 displays comparative cooling and subsequent heating DSC thermograms of these polymers at a rate of 10 °C min^{-1} under N_2. The presence of isotactic alcohol units slightly increases the T_g to 53 °C, but dramatically changes the semi-crystalline properties. **HP2S−OH(96)** has a T_m = 189 °C and ΔH_m = 101 J g^{-1} which are 65 °C and 71 J g^{-1} higher than the atactic analogue, and much higher than any of the atactic samples in Table 1. To date, T_m values ≥ 190 °C have only been seen from systems with a VOH content exceeding 80 mol %,[33,38] which is double the VOH content of our isotactic material. This is important to note because the VOH content can have a dramatic influence on the material's barrier properties.[32,55] Another notable feature is the sharp crystallization exotherm upon cooling (T_c = 161 °C, ΔH_c = 94 J g^{-1}) suggesting that the precise isotactic microstructure is leading to kinetically fast nucleation and growth of crystalline regions, which are features of defect-free linear, flexible homopolymers. Further analysis and insights on comparative structural details and crystallization kinetics are under investigation. **HP2R−OH(96)** also had a high T_m of 190 °C, similar to the *S* analogue (Figure S61). The ΔH_m (58.8 J g^{-1}) was reduced compared to **HP2S−OH** for reasons currently unknown.

X-ray Scattering Analysis. The structural differences between crystallites formed from the melt of isotactic and atactic samples are evaluated from WAXD and SAXS patterns of isothermally crystallized samples collected at room temperature. The isothermal crystallization was conducted in the DSC using Al pans, as mentioned in the experimental section. The samples were heated at 210 °C for 5 min to erase thermal history and cooled at 40 °C min^{-1} to a crystallization temperature of 170 °C (isotactic sample) or 116 °C (atactic sample). After complete isothermal transformation, the temperature was lowered at a rate of 40 °C min^{-1} to 20 °C, and the sample removed from the Al pan for collection of X-ray patterns. Rather than a dynamic cooling from the melt to room temperature at 10 °C min^{-1}, the above isothermal crystallization is chosen to maximize the three-dimensional crystal packing.

For these structural analyses, the atactic sample with the highest regioregularity was chosen because though all atactic samples of Table 1 display identical WAXD patterns, **HP2−OH(99)** was the only sample with an observable SAXS scattering peak associated with correlated symmetry between lamellar crystallites (Figure 4b). The WAXD patterns of **HP2−**

https://doi.org/10.1021/acs.macromol.2c01090
Macromolecules 2022, 55, 6841−6851

Table 1. Characterization and Thermal Properties of Synthesized Atactic and Isotactic Polymers

sample ID	M_n[a] (kg mol^{-1})	Đ[b]	%HT[c]	T_g[d] (°C)	T_m[d] (°C)	ΔH_m[d] (J g^{-1})	T_c[e] (°C)	ΔH_c[e] (J g^{-1})	T_d[f] (°C)
HP2−OH(77)	27	2.13	77	40[g]	96	27.5	80	23.4	
HP2−OH(96)	125	1.50	96	46	125	29.7	80	18.8	365
HP2−OH(97)	65	1.56	97	46	124	33.7	76	16.9	
HP2−OH(99)	410	1.60	99	48	137	40.2	106	37.8	
HP2S−OH(96)	110	1.56	96	53	189	101.0	161	94.0	395
HP2R−OH(96)	143	1.61	96	47	190	58.8	157	58.5	385

[a]Calculated number average molar mass (M_n) based on SEC analysis of the respective TBS protected version of the polymer and corrected for quantitative loss of TBS groups. [b]Dispersity (Đ) determined by SEC analysis on TBS protected versions of the polymer. [c]Percent HT regioregularity determined by peak deconvolution analysis of methine proton signals from ^{1}H NMR in $CDCl_3$. [d]Glass transition temperature (T_g), crystalline melting temperature (T_m), and enthalpy of melting (ΔH_m) determined by DSC analysis upon second heating at 10 °C min^{-1}. [e]Crystallization temperature (T_c) and enthalpy (ΔH_c) determined by DSC analysis upon cooling from the melt at 10 °C min^{-1}. [f]Decomposition temperature determined as the point of 5% mass loss upon heating by TGA analysis at 10 °C min^{-1} under argon. [g]Broad transition in a temperature range of 36−46 °C.

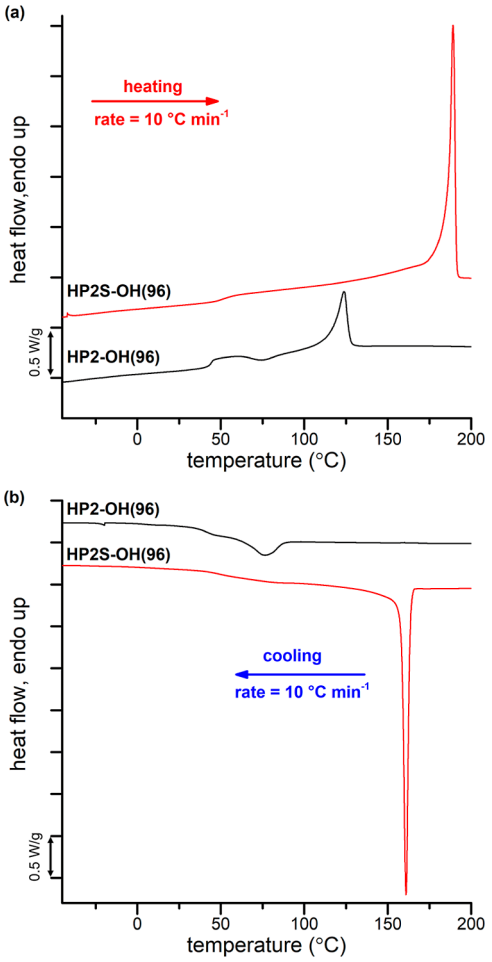

Figure 3. Comparative DSC thermograms of atactic **HP2−OH(96)** (black) and isotactic **HP2S−OH(96)** (red) upon the second cycle of (a) heating and (b) cooling at 10 °C min^{-1} under N_2.

OH(99) and **HP2S−OH(96)**, shown in Figure 4a, display a major reflection at 1.44 and 1.49 Å^{-1}, respectively, with an amorphous halo shoulder at ∼1.40 Å^{-1} and other low intensity reflections at higher q values. Both patterns are remarkably similar inferring chain packing in the same type of unit cell, independent of tacticity. In contrast, the WAXD patterns of atactic and highly isotactic PVA are different and it was speculated that this may be due to a preferential intramolecular hydrogen bonding for the isotactic polymer and intermolecular for atactic PVA.[56,57]

The reflections at q = 0.92 and 1.0 Å^{-1} found for both polymers as shown in Figure 4a correspond to periodicities of 6.8 and 6.3 Å respectively, which are very close to 6.35 Å, the calculated length for the all-trans repeating unit, indicating that both polymers pack in alcohol−alcohol layered crystallites. Because consecutive OH units in the chain are too far for effective intramolecular hydrogen bonding, one can infer a molecular crystalline arrangement for both polymers similar to the intermolecular O···H hydrogen bonding proposed for atactic PVA.[57−62] Although establishing the type of unit cell requires analysis of oriented fiber patterns, the reflection at q = 1.0 Å^{-1} corresponds directly to the expected all-trans repeat unit distance, hence it is consistent with the (002) layer plane. The foreseen molecular path in the crystal structure is schematically represented in Figure 5 where the different length scales that can be extracted from WAXD and SAXS patterns are indicated.

The fractional levels of crystallinity (X_c) of **HP2−OH(99)** and **HP2S−OH(96)** were estimated by a peak-fitting analysis of the major crystalline diffraction and of the distinctive amorphous halo at q = 1.4 Å^{-1}, as shown in the insets of Figure 4a. The resulting values of X_c are 0.39 and 0.20 for the isotactic and atactic polymer, respectively (Table 2). If higher q reflections are included in the analysis, the crystallinity content increases by ∼ 5%. Clearly, even when both systems may pack in the same unit cell and form OH-layered crystallites, the atactic configuration drastically restricts development of crystallinity, which is about half the level acquired by the isotactic analogue.

The Lorentz-corrected SAXS patterns are shown in Figure 4b. Shallow and broad scattering peaks are found at 0.035 and 0.048 Å^{-1}, which correspond to long periods (L) of 180 and 131 Å for the atactic and isotactic polymer, respectively (Table 2). Unfortunately, the high signal-to-noise of the SAXS patterns prevented a reliable correlation function analysis to compare the core thicknesses of the lamellar crystallites. Moreover, because polarized optical micrographs of these samples (Figure S63) indicate a crystalline morphology of aggregates pervading the whole sample volume, we estimated the crystal thickness as the product of L and X_c, the latter obtained by peak fitting analysis of the WAXD patterns as described above. The estimated crystal thicknesses (l_c) for the isotactic and atactic samples are 51 and 36 Å, respectively (Table 2), corresponding to ∼8 and ∼6 monomer repeats

https://doi.org/10.1021/acs.macromol.2c01090
Macromolecules 2022, 55, 6841−6851

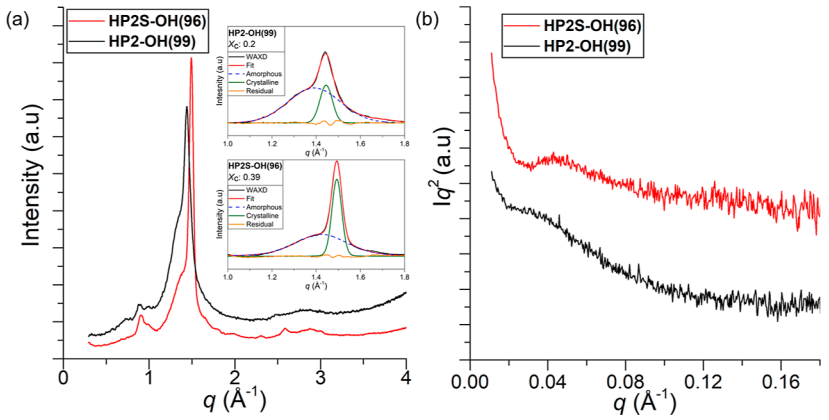

Figure 4. (a) WAXD patterns of isothermally crystallized **HP2−OH(99)** (black) and **HP2S−OH(96)** (red) taken at 24 °C. (b) Lorentz-corrected SAXS patterns of the same polymers. Inset in (a) shows the peak-fitting analysis of the WAXD patterns used to determine the degree of crystallinity (X_c).

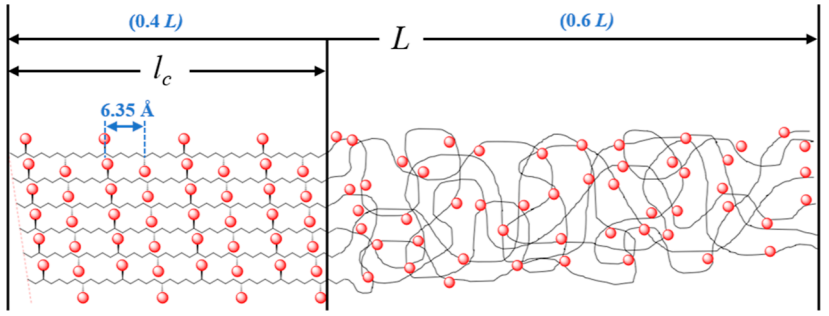

Figure 5. Schematic representation of the isotactic precision polymer with molecular packing and the different length scales of crystalline and amorphous regions extracted from WAXD and SAXS data. Red spheres represent alcohol pendants.

Table 2. X-ray Scattering Data Comparison of Atactic and Isotactic Samples

ID	$q_{(SAXS)}$[a] (Å^{-1})	L[b] (Å)	X_c[c]	l_c[d] (Å)	$q_{(WAXD)}$[e] (Å^{-1})
HP2−OH(99)	0.035	180	0.20	35.9	1.44
HP2S−OH(96)	0.048	131	0.39	51.1	1.49

[a]Maximum SAXS peak (q). [b]Lamellar long period determined from $L = 2\pi/q_{(SAXS)}$. [c]Fractional crystallinity based on peak-fitting analysis of WAXD patterns as shown in Figure 4. [d]Core crystal thickness estimated as $L \cdot X_c$. [e]Main reflection from the WAXD patterns.

(layers) normal to the lamellar basal surface. Much thicker crystals for the isotactic polymer are also reflected by the narrower WAXD pattern as shown in Figure 4a.

Of interest from the WAXD patterns is the shift to lower q of the main reflection in the pattern of the atactic polymer, inferring a more expanded (less dense) crystal lattice than the lattice of the isotactic analogue. This inference, in combination with SAXS structural data, corroborate that though the crystal unit cell may be equivalent for the two melt-crystallized polymers, the highly isotactic molecule confers more densely packed crystallites. The densification of the isotactic sample is arguably due to a more efficient intermolecular hydrogen bonding facilitated by the stereoregularity of the alcohol pendant. Conversely, lacking such symmetry in the configuration of consecutive alcohol pendants in the atactic molecule, crystallization is restricted as shown by a dramatic decrease of level of crystallinity and by thinner and more defective crystallites.

CONCLUSIONS

For the first time, a semi-crystalline polyolefin featuring an isotactic pendant alcohol at each and every fifth carbon along a linear polyethylene backbone was synthesized. These materials were made with high molar mass (>100 kg mol^{-1}) and moderate dispersity (1.5−2.1) through cold-temperature ROMP of bulky, TBS-protected, 2-cyclopentenol followed by olefin hydrogenation and post-polymerization deprotection of the alcohol pendants. Although the molar masses and dispersities achieved were uncontrolled, a high degree of HT regioregularity and high *trans* content, coupled with an enantiopure monomer feedstock, produced the most microstructurally precise polypentenamers to date.[31] Following saturation and deprotection, crystalline properties were investigated and compared with atactic analogues with identical composition, yet varying degrees of regioregularity. These precision atactic and isotactic materials with ∼96% HT regioregularity have a $T_g \approx 50$ °C, yet the isotactic has a $T_m \approx 190$ °C, which is 60 °C higher than any of the atactic analogues. Although both types display very similar WAXD patterns, indicating near-equivalent unit cells, the isotactic polymer develops double the degree of crystallinity (>40%), and thicker crystallites over its atactic counterparts, and thermal stability >385 °C. In addition to fundamental discoveries pertaining to the structure−property relationships and crystallization behavior of materials with isotactic branches at unexplored periodicities, these materials may also present new discoveries on how precise microstructure influences mechanical and barrier properties. Such will be the focus of future investigations.

https://doi.org/10.1021/acs.macromol.2c01090
Macromolecules 2022, 55, 6841−6851

■ ASSOCIATED CONTENT

Supporting Information

The Supporting Information is available free of charge at https://pubs.acs.org/doi/10.1021/acs.macromol.2c01090.

Additional synthetic procedures and characterization data (NMR, SEC, DSC, TGA, POM) (PDF)

■ AUTHOR INFORMATION

Corresponding Author

Justin G. Kennemur − *Department of Chemistry and Biochemistry, Florida State University, Tallahassee, Florida 32306, United States;* orcid.org/0000-0002-2322-0386; Email: jkennemur@fsu.edu

Authors

Gina A. Guillory − *Department of Chemistry and Biochemistry, Florida State University, Tallahassee, Florida 32306, United States*

Stephanie F. Marxsen − *Department of Chemical and Biomedical Engineering College of Engineering, Florida A&M University−Florida State University (FAMU-FSU), Tallahassee, Florida 32310, United States;* orcid.org/0000-0002-7766-8768

Rufina G. Alamo − *Department of Chemical and Biomedical Engineering College of Engineering, Florida A&M University−Florida State University (FAMU-FSU), Tallahassee, Florida 32310, United States;* orcid.org/0000-0002-3061-499X

Complete contact information is available at: https://pubs.acs.org/10.1021/acs.macromol.2c01090

Author Contributions

The manuscript was written through contributions of all authors. All authors have given approval to the final version of the manuscript.

Notes

The authors declare no competing financial interest.

■ ACKNOWLEDGMENTS

J.G.K. and G.A.G. acknowledge the National Science Foundation, DMR Polymer Program CAREER Grant 1750852, for financial support of this work. R.G.A. and S.F.M. acknowledge funding by the National Science Foundation, Polymer Program DMR 1607786. We are indebted to the High-Performance Materials Institute (HPMI) of Florida State University for access to local X-ray instrumentation. Portions of this research used resources provided by the NMR Facility (FSU075000NMR) and the Materials Characterization Laboratory (FSU075000MAC) at the FSU Department of Chemistry and Biochemistry. We thank Prof. Ralm Ricarte for discussion on X-ray scattering data and Umicore for donating some of the HG2 catalyst (Umicore M720) used in this research.

■ REFERENCES

(1) Teator, A. J.; Varner, T. P.; Knutson, P. C.; Sorensen, C. C.; Leibfarth, F. A. 100th Anniversary of Macromolecular Science Viewpoint: The Past, Present, and Future of Stereocontrolled Vinyl Polymerization. *ACS Macro Lett.* **2020**, *9*, 1638−1654.

(2) Doerr, A. M.; Burroughs, J. M.; Gitter, S. R.; Yang, X.; Boydston, A. J.; Long, B. K. Advances in Polymerizations Modulated by External Stimuli. *ACS Catal.* **2020**, *10*, 14457−14515.

(3) Walsh, D. J.; Hyatt, M. G.; Miller, S. A.; Guironnet, D. Recent Trends in Catalytic Polymerizations. *ACS Catal.* **2019**, *9*, 11153−11188.

(4) Chen, C. Designing catalysts for olefin polymerization and copolymerization: beyond electronic and steric tuning. *Nat. Rev. Chem.* **2018**, *2*, 6−14.

(5) Liu, P.; Liu, W.; Wang, W.-J.; Li, B.-G.; Zhu, S. A Comprehensive Review on Controlled Synthesis of Long-Chain Branched Polyolefins: Part 1, Single Catalyst Systems. *Macromol. React. Eng.* **2016**, *10*, 156−179.

(6) Soller, B. S.; Zhang, N.; Rieger, B. Catalytic Precision Polymerization: Rare Earth Metal-Mediated Synthesis of Homopolymers, Block Copolymers, and Polymer Brushes. *Macromol. Chem. Phys.* **2014**, *215*, 1946−1962.

(7) Nakamura, A.; Anselment, T. M. J.; Claverie, J.; Goodall, B.; Jordan, R. F.; Mecking, S.; Rieger, B.; Sen, A.; van Leeuwen, P. W. N. M.; Nozaki, K. Ortho-Phosphinobenzenesulfonate: A Superb Ligand for Palladium-Catalyzed Coordination−Insertion Copolymerization of Polar Vinyl Monomers. *Acc. Chem. Res.* **2013**, *46*, 1438−1449.

(8) Chen, E. Y. X. Coordination Polymerization of Polar Vinyl Monomers by Single-Site Metal Catalysts. *Chem. Rev.* **2009**, *109*, 5157−5214.

(9) Chum, P. S.; Swogger, K. W. Olefin polymer technologies-History and recent progress at The Dow Chemical Company. *Prog. Polym. Sci.* **2008**, *33*, 797−819.

(10) Domski, G. J.; Rose, J. M.; Coates, G. W.; Bolig, A. D.; Brookhart, M. Living alkene polymerization: New methods for the precision synthesis of polyolefins. *Prog. Polym. Sci.* **2007**, *32*, 30−92.

(11) Coates, G. W. Precise Control of Polyolefin Stereochemistry Using Single-Site Metal Catalysts. *Chem. Rev.* **2000**, *100*, 1223−1252.

(12) Ogba, O. M.; Warner, N. C.; O'Leary, D. J.; Grubbs, R. H. Recent advances in ruthenium-based olefin metathesis. *Chem. Soc. Rev.* **2018**, *47*, 4510−4544.

(13) Caire da Silva, L.; Rojas, G.; Schulz, M. D.; Wagener, K. B. Acyclic diene metathesis polymerization: History, methods and applications. *Prog. Polym. Sci.* **2017**, *69*, 79−107.

(14) Grubbs, R. H.; Khosravi, E. *Handbook of Metathesis*, 2nd Edition; Wiley-VCH: Weinheim, Germany, 2015.

(15) Grubbs, R. H.. *Handbook of Metathesis*; Wiley-VCH: Weinheim, Germany, 2003; Vol. *3*.

(16) Pearce, A. K.; Foster, J. C.; O'Reilly, R. K. Recent developments in entropy-driven ring-opening metathesis polymerization: Mechanistic considerations, unique functionality, and sequence control. *J. Polym. Sci., Part A: Polym. Chem.* **2019**, *57*, 1621−1634.

(17) Neary, W. J.; Kennemur, J. G. Polypentenamer Renaissance: Challenges and Opportunities. *ACS Macro Lett.* **2019**, *8*, 46−56.

(18) Atallah, P.; Wagener, K. B.; Schulz, M. D. ADMET: The Future Revealed. *Macromolecules* **2013**, *46*, 4735−4741.

(19) Mutlu, H.; de Espinosa, L. M.; Meier, M. A. R. Acyclic diene metathesis: a versatile tool for the construction of defined polymer architectures. *Chem. Soc. Rev.* **2011**, *40*, 1404−1445.

(20) Kobayashi, S.; Pitet, L. M.; Hillmyer, M. A. Regio- and Stereoselective Ring-Opening Metathesis Polymerization of 3-Substituted Cyclooctenes. *J. Am. Chem. Soc.* **2011**, *133*, 5794−5797.

(21) Martinez, H.; Miró, P.; Charbonneau, P.; Hillmyer, M. A.; Cramer, C. J. Selectivity in Ring-Opening Metathesis Polymerization of Z-Cyclooctenes Catalyzed by a Second-generation Grubbs Catalyst. *ACS Catal.* **2012**, *2*, 2547−2556.

(22) Zhang, J. H.; Matta, M. E.; Martinez, H.; Hillmyer, M. A. Precision Vinyl Acetate/Ethylene (VAE) Copolymers by ROMP of Acetoxy-Substituted Cyclic Alkenes. *Macromolecules* **2013**, *46*, 2535−2543.

(23) Kobayashi, S.; Fukuda, K.; Kataoka, M.; Tanaka, M. Regioselective Ring-Opening Metathesis Polymerization of 3-Substituted Cyclooctenes with Ether Side Chains. *Macromolecules* **2016**, *49*, 2493−2501.

(24) Liu, F.; Xu, N.; Ling, L.; Hu, J.; Zhang, H. Regio- and stereoselective ring-opening metathesis polymerization of 3-ferrocenyl

substituted cyclooctenes and copolymerization with norbornene derivatives. *Eur. Polym. J.* **2020**, *124*, 109472.
(25) Osawa, K.; Kobayashi, S.; Tanaka, M. Synthesis of Sequence-Specific Polymers with Amide Side Chains via Regio-/Stereoselective Ring-Opening Metathesis Polymerization of 3-Substituted cis-Cyclooctene. *Macromolecules* **2016**, *49*, 8154−8161.
(26) Sonoda, T.; Kobayashi, S.; Tanaka, M. Periodically Functionalized Linear Polyethylene with Tertiary Amino Groups via Regioselective Ring-Opening Metathesis Polymerization. *Macromolecules* **2021**, *54*, 2862−2872.
(27) Li, M.; Cui, F.; Li, Y.; Tao, Y.; Wang, X. Crystalline Regio-/Stereoregular Glycine-Bearing Polymers from ROMP: Effect of Microstructures on Materials Performances. *Macromolecules* **2016**, *49*, 9415−9424.
(28) Zhang, J. H.; Matta, M. E.; Hillmyer, M. A. Synthesis of Sequence-Specific Vinyl Copolymers by Regioselective ROMP of Multiply Substituted Cyclooctenes. *ACS Macro Lett.* **2012**, *1*, 1383−1387.
(29) Guillory, G. A.; Kennemur, J. G. Investigating the effects of bulky allylic substituents on the regioregularity and thermodynamics of ROMP on cyclopentene. *Eur. Polym. J.* **2019**, *120*, 109251.
(30) Brits, S.; Neary, W. J.; Palui, G.; Kennemur, J. G. A new echelon of precision polypentenamers: highly isotactic branching on every five carbons. *Polym. Chem.* **2018**, *9*, 1719−1727.
(31) Kennemur, J. G. Cyclopentene monomers and methods of polymerization. U.S. Patent 11,136,426 B2, 2021
(32) Mokwena, K. K.; Tang, J. Ethylene Vinyl Alcohol: A Review of Barrier Properties for Packaging Shelf Stable Foods. *Crit. Rev. Food Sci.* **2012**, *52*, 640−650.
(33) Mori, Y.; Sumi, H.; Hirabayashi, T.; Inai, Y.; Yokota, K. Synthesis of Sequence-Ordered Copolymers. 4. Glass Transition and Melting Temperatures of Sequence-Ordered and Unordered Ethylene-Vinyl Alcohol and Ethylene-Vinyl Acetate Copolymers. *Macromolecules* **1994**, *27*, 1051−1056.
(34) Ramakrishnan, S.; Chung, T. C. Poly(5-hydroxyoctenylene) and its derivatives: synthesis via metathesis polymerization of an organoborane monomer. *Macromolecules* **1990**, *23*, 4519−4524.
(35) Ramakrishnan, S. Well-defined ethylene-vinyl alcohol copolymers via hydroboration: control of composition and distribution of the hydroxyl groups on the polymer backbone. *Macromolecules* **1991**, *24*, 3753−3759.
(36) Herz, K.; Imbrich, D. A.; Unold, J.; Xu, G. J.; Speiser, M.; Buchmeiser, M. R. Functional ROMP-Derived Poly(cyclopentene)s. *Macromol. Chem. Phys.* **2013**, *214*, 1522−1527.
(37) Hillmyer, M. A.; Laredo, W. R.; Grubbs, R. H. Ring-Opening Metathesis Polymerization of Functionalized Cyclooctenes by a Ruthenium-Based Metathesis Catalyst. *Macromolecules* **1995**, *28*, 6311−6316.
(38) Scherman, O. A.; Kim, H. M.; Grubbs, R. H. Synthesis of Well-Defined Poly((vinyl alcohol)2-alt-methylene) via Ring-Opening Metathesis Polymerization. *Macromolecules* **2002**, *35*, 5366−5371.
(39) Scherman, O. A.; Walker, R.; Grubbs, R. H. Synthesis and Characterization of Stereoregular Ethylene-Vinyl Alcohol Copolymers Made by Ring-Opening Metathesis Polymerization. *Macromolecules* **2005**, *38*, 9009−9014.
(40) Valenti, D. J.; Wagener, K. B. Direct Synthesis of Well-Defined Alcohol-Functionalized Polymers via Acyclic Diene Metathesis (ADMET) Polymerization. *Macromolecules* **1998**, *31*, 2764−2773.
(41) Li, Z.-L.; Lv, A.; Li, L.; Deng, X.-X.; Zhang, L.-J.; Du, F.-S.; Li, Z.-C. Periodic ethylene-vinyl alcohol copolymers via ADMET polymerization: Synthesis, characterization, and thermal property. *Polymer* **2013**, *54*, 3841−3849.
(42) Santonja-Blasco, L.; Zhang, X.; Alamo, R. G. Crystallization of Precision Ethylene Copolymers. In *Polymer Crystallization I: From Chain Microstructure to Processing*; Auriemma, F., Alfonso, G. C., de Rosa, C., Eds.; Springer International Publishing: Cham, 2017, pp 133−182.
(43) Thompson, D.; Yamakado, R.; Wagener, K. B. Extending the Methylene Spacer Length of ADMET Hydroxy-Functionalized Polymers. *Macromol. Chem. Phys.* **2014**, *215*, 1212−1217.
(44) Tuba, R.; Al-Hashimi, M.; Bazzi, H. S.; Grubbs, R. H. One-Pot Synthesis of Poly(vinyl alcohol) (PVA) Copolymers via Ruthenium Catalyzed Equilibrium Ring-Opening Metathesis Polymerization of Hydroxyl Functionalized Cyclopentene. *Macromolecules* **2014**, *47*, 8190−8195.
(45) Trost, B. M.; Van Vranken, D. L.; Bingel, C. A modular approach for ligand design for asymmetric allylic alkylations via enantioselective palladium-catalyzed ionizations. *J. Am. Chem. Soc.* **1992**, *114*, 9327−9343.
(46) Fuchs, S.; Berl, V.; Lepoittevin, J.-P. A Highly Stereoselective Divergent Synthesis of Bicyclic Models of Photoreactive Sesquiterpene Lactones. *Eur. J. Org. Chem.* **2007**, *2007*, 1145−1152.
(47) Lüssem, B. J.; Gais, H. J. Palladium-catalyzed deracemization of allylic carbonates in water with formation of allylic alcohols: Hydrogen carbonate ion as nucleophile in the palladium-catalyzed allylic substitution and kinetic resolution. *J. Am. Chem. Soc.* **2003**, *125*, 6066−6067.
(48) Martinez, H.; Zhang, J.; Kobayashi, S.; Xu, Y.; Pitet, L. M.; Matta, M. E.; Hillmyer, M. A. Functionalized regio-regular linear polyethylenes from the ROMP of 3-substituted cyclooctenes. *Appl. Petrochem. Res.* **2015**, *5*, 19−25.
(49) Winkler, M.; Steinbiß, M.; Meier, M. A. R. A more sustainable Wohl−Ziegler bromination: Versatile derivatization of unsaturated FAMEs and synthesis of renewable polyamides. *Eur. J. Lipid Sci. Technol.* **2014**, *116*, 44−51.
(50) Hoye, T. R.; Jeffrey, C. S.; Shao, F. Mosher ester analysis for the determination of absolute configuration of stereogenic (chiral) carbinol carbons. *Nat. Protoc.* **2007**, *2*, 2451.
(51) Sita, L. R. Main-Chain Chiral Polymers from β-Citronellene via Tandem Diene Metathesis Cyclization/Ring-Opening Metathesis Polymerization. *Macromolecules* **1995**, *28*, 656−657.
(52) Ohgi, H.; Sato, T.; Hu, S.; Horii, F. Highly isotactic poly(vinyl alcohol) derived from tert-butyl vinyl ether. Part IV. Some physical properties, structure and hydrogen bonding of highly isotactic poly(vinyl alcohol) films. *Polymer* **2006**, *47*, 1324−1332.
(53) Neary, W. J.; Kennemur, J. G. A Precision Ethylene-Styrene Copolymer with High Styrene Content from Ring-Opening Metathesis Polymerization of 4-Phenylcyclopentene. *Macromol. Rapid Commun.* **2016**, *37*, 975−979.
(54) Alamo, R. G.; Chan, E. K. M.; Mandelkern, L.; Voigt-Martin, I. G. Influence of molecular weight on the melting and phase structure of random copolymers of ethylene. *Macromolecules* **1992**, *25*, 6381−6394.
(55) Maes, C.; Luyten, W.; Herremans, G.; Peeters, R.; Carleer, R.; Buntinx, M. Recent Updates on the Barrier Properties of Ethylene Vinyl Alcohol Copolymer (EVOH): A Review. *Polym. Rev.* **2018**, *58*, 209−246.
(56) Ohgi, H.; Sato, T. Preparation of highly isotactic poly(vinyl alcohol). *Macromolecules* **1993**, *26*, 559−560.
(57) Murahashi, S.; Yûcki, H.; Sano, T.; Yonemura, U.; Tadokoro, H.; Chatani, Y. Isotactic polyvinyl alcohol. *J. Polym. Sci.* **1962**, *62*, S77−S81.
(58) Bunn, C. W. Crystal Structure of Polyvinyl Alcohol. *Nature* **1948**, *161*, 929−930.
(59) Mooney, R. C. L. An X-Ray Study of the Structure of Polyvinyl Alcohol. *J. Am. Chem. Soc.* **1941**, *63*, 2828−2832.
(60) Ricciardi, R.; Auriemma, F.; De Rosa, C.; Lauprêtre, F. X-ray Diffraction Analysis of Poly(vinyl alcohol) Hydrogels, Obtained by Freezing and Thawing Techniques. *Macromolecules* **2004**, *37*, 1921−1927.
(61) Assender, H. E.; Windle, A. H. Crystallinity in poly(vinyl alcohol). 1. An X-ray diffraction study of atactic PVOH. *Polymer* **1998**, *39*, 4295−4302.
(62) Assender, H. E.; Windle, A. H. Crystallinity in poly(vinyl alcohol) 2. Computer modelling of crystal structure over a range of tacticities. *Polymer* **1998**, *39*, 4303−4312.

https://doi.org/10.1021/acs.macromol.2c01090
Macromolecules 2022, 55, 6841−6851